INTERNATIONAL JOURNAL FOR NUMERICAL METHODS IN ENGINEERING
Int. J. Numer. Meth. Engng 2003; **56**:185–209 (DOI: 10.1002/nme.554)

Stabilized finite element method for viscoplastic flow: formulation with state variable evolution

Antoinette M. Maniatty[1,*,†] and Yong Liu[2]

[1]*Department of Mechanical, Aerospace and Nuclear Engineering, Rensselaer Polytechnic Institute, Troy, NY 12180, U.S.A.*
[2]*Technology CAD Department, Fairchild Semiconductor, South Portland, ME 04106, U.S.A.*

SUMMARY

A stabilized, mixed finite element formulation for modelling viscoplastic flow, which can be used to model approximately steady-state metal-forming processes, is presented. The mixed formulation is expressed in terms of the velocity, pressure and state variable fields, where the state variable is used to describe the evolution of the material's resistance to plastic flow. The resulting system of equations has two sources of well-known instabilities, one due to the incompressibility constraint and one due to the convection-type state variable equation. Both of these instabilities are handled by adding mesh-dependent stabilization terms, which are functions of the Euler–Lagrange equations, to the usual Galerkin method. Linearization of the weak form is derived to enable a Newton–Raphson implementation into an object-oriented finite element framework. A progressive solution strategy is used for improving convergence for highly non-linear material behaviour, typical for metals. Numerical experiments using the stabilization method with hierarchic shape functions for the velocity, pressure and state variable fields in viscoplastic flow and metal-forming problems show that the stabilized finite element method is effective and efficient for non-linear steady forming problems. Finally, the results are discussed and conclusions are inferred.

KEY WORDS: stabilized finite element method; viscoplastic flow; metal forming

1. INTRODUCTION

Many important forming processes, such as rolling and extrusion, can be effectively modelled by assuming that the process is approximately steady state and modelling the material as purely viscoplastic, i.e. neglecting elasticity, see, for example, the works of Dawson [1], Kobayashi *et al.* [2] and Maniatty and Chen [3]. While such formulations cannot predict elastic effects,

*Correspondence to: Antoinette M. Maniatty, Department of Mechanical, Aerospace and Nuclear Engineering, Rensselaer Polytechnic Institute, 110 8th Street, Troy, NY 12180-3590, U.S.A.
†E-mail: maniaa@rpi.edu

Contract/grant sponsor: National Science Foundation and U.S. Department of Defense—Department of the Air Force, Wright Laboratory; contract/grant number: DMI-9634920

Received 26 September 2001
Revised 1 March 2002

such as residual stresses, they can provide useful information about the flow field, stresses during deformation, forces required for forming, and evolution of the material state.

In the modelling of forming processes using the finite element method, especially three-dimensional processes, it is important to have a flexible method to balance accuracy and efficiency. Galerkin methods applied to incompressible material behaviour, typical for metals at large strains, in the setting of a mixed finite element method must fulfil the Ladyzenskaya–Babuska–Brezzi (LBB) condition to achieve unique solvability, convergence and robustness [4]. This places severe restrictions on the choice of the solution space. Without balancing the interpolation functions according to the LBB condition, large errors or oscillations may appear in the solution. Stabilized finite element methods avoid these limitations providing greater flexibility in choosing interpolation functions.

Galerkin methods applied to convection-dominated problems also frequently result in non-physical oscillations in the solution, see, for example, References [5, 6]. Several procedures have been proposed to handle convection-dominated problems. The most common methods are streamline upwind Petrov–Galerkin (SUPG) methods [7–11] and discontinuous Galerkin methods [12, 13]. In SUPG methods, the weighting function used in the finite element formulation is not the same as the interpolation function, but rather is the interpolation function plus an additional mesh-dependent term. The form of the additional function can be derived in a number of different ways with similar results. In discontinuous Galerkin methods, discontinuous interpolation functions are used and interelement continuity conditions are satisfied in a weak sense. Stabilized finite element methods have also been successfully applied to convection-dominated problems and result in a formulation identical to that obtained with SUPG methods.

Stabilized finite element formulations, in general, consist of adding mesh-dependent terms to the usual Galerkin method. Those terms are functions of the residuals of the Euler–Lagrange equations evaluated elementwise. From the construction, it follows that consistency is not affected since the exact solution satisfies both the Galerkin term and the additional terms. Stabilized finite element methods have been used to handle instabilities due to incompressibility in linear problems in both solid and fluid mechanics, for example, see References [14, 15]. Recently, Klaas *et al.* [16] have applied the stabilized finite element method to hyperelasticity, and the results show the effectiveness of this method for nearly incompressible, non-linear large deformation problems. Maniatty and co-workers [17] have presented a stabilized mixed finite element formulation for solid viscoplastic flow problems. However, in that work, they did not study the state variable evolution, which may also need stabilization in an Eulerian formulation because of the convection term. Stabilized finite element methods have been shown to be effective for convection-dominated problems, see, for example, References [6, 18].

In this paper, the stabilized finite element method is extended to handle a three-field (velocity, pressure and state variable fields), steady, viscoplastic flow problem. The goal for the remainder of this paper consists of developing a comprehensive presentation for solving problems involving very non-linear material constitutive relations with state variable evolution. The next sections are organized as follows. First, some background is given and the basic notation and terminology for the governing equations are established. Next, a brief review of the stabilized formulation for handling the incompressible viscoplastic flow problem in an Eulerian configuration is given. Then, the stabilized formulation for handling the convective state variable evolution equation is derived. The three-field, stabilized formulation is linearized to allow an implementation in a Newton–Raphson scheme.

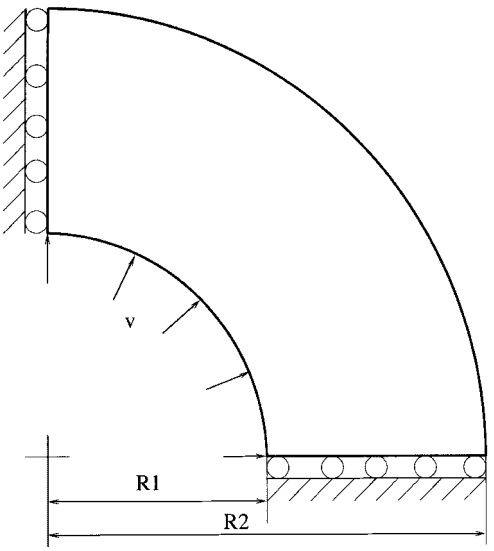

Figure 1. Hollow cylinder subjected to radial velocity.

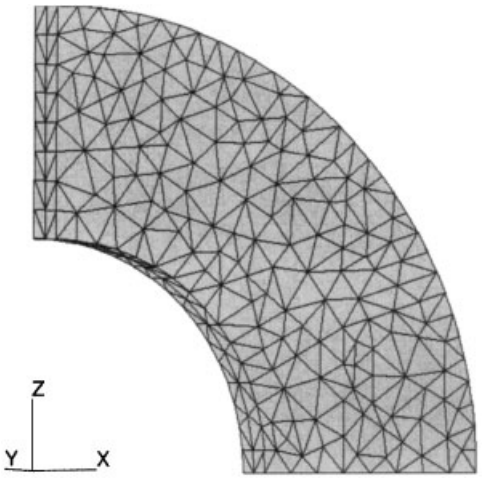

Figure 2. Mesh of hollow cylinder model.

A progressive solution strategy is described, which is used to improve convergence. Applications to forming problems are investigated. Finally, the results are discussed and conclusions are inferred.

2. GOVERNING EQUATIONS

Consider a three-dimensional domain B with boundary ∂B where the material being deformed is flowing steadily through the domain. The material is assumed to be isotropic, isochoric and viscoplastic. In this formulation, elasticity is neglected, thus quantities such as residual stresses cannot be determined. The governing equations for the boundary-value problem on B are

$$\operatorname{div} \boldsymbol{\sigma} = 0 \quad \text{in } B \tag{1}$$

$$\operatorname{tr}(\mathbf{D}) = \operatorname{div} \mathbf{v} = 0 \quad \text{in } B \tag{2}$$

$$\boldsymbol{\sigma}' = 2\mu \mathbf{D} \quad \text{in } B \tag{3}$$

$$\bar{\sigma} = f(\dot{\varepsilon}, s) \quad \text{in } B \tag{4}$$

$$\dot{s} = g(\dot{\varepsilon}, s) = \nabla s \cdot \mathbf{v} \quad \text{in } B \tag{5}$$

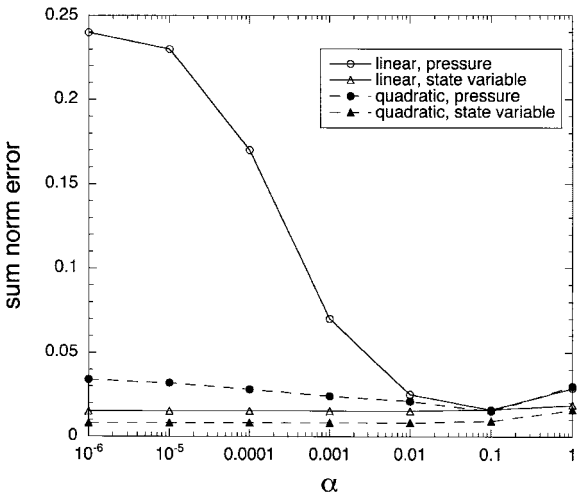

Figure 3. Error in the pressure and state variable fields as a function of stabilization parameter α.

Table I. Velocity comparison (power law with $m = 0.05$ and $\alpha = 0.1$, $\beta = 1.0$).

Position (r)	1.0	1.25	1.5	1.75	2.0
v_{Exact}	0.1	0.08	0.06667	0.05714	0.05
v_{FEM}	0.1	0.07970	0.06645	0.05706	0.04996

where $\boldsymbol{\sigma}$ is the Cauchy stress tensor, $\mathbf{D} = \text{sym}(\nabla \mathbf{v})$ is the rate of deformation tensor, $\mathbf{v}$ is the velocity vector, s is the state variable and ∇ is the gradient operator on B. Furthermore,

$$\dot{\varepsilon} = \sqrt{\tfrac{2}{3}\mathbf{D}:\mathbf{D}}, \quad \bar{\sigma} = \sqrt{\tfrac{3}{2}\boldsymbol{\sigma}':\boldsymbol{\sigma}'}, \quad \boldsymbol{\sigma}' = \boldsymbol{\sigma} - \tfrac{1}{3}(\text{tr}\,\boldsymbol{\sigma})\mathbf{I} = \boldsymbol{\sigma} + p\mathbf{I}$$

where p is the pressure. Equation (1) is the equilibrium equation, Equation (2) enforces incompressibility, Equations (3) and (4) are the constitutive law flow rules relating the rate of deformation to the stress, and Equation (5) is the evolution equation for state variable s where the second right-hand side is a purely convective term and is due to the steady flow assumption. In addition, from the above equations the effective viscosity is

$$\mu = \frac{f(\dot{\varepsilon}, s)}{3\dot{\varepsilon}} \tag{6}$$

The associated boundary conditions are

$$\mathbf{v} = \hat{\mathbf{v}} \quad \text{on } \partial B_{\text{D}} \tag{7}$$

$$\boldsymbol{\sigma} \cdot \mathbf{n} = \hat{\mathbf{t}} \quad \text{on } \partial B_{\text{N}} \tag{8}$$

$$\mathbf{e}_{\text{T}} \cdot \boldsymbol{\sigma} \cdot \mathbf{n} = \eta(\mathbf{v}_{\text{o}} - \mathbf{v}) \cdot \mathbf{e}_{\text{T}} \quad \text{on } \partial B_{\text{F}} \tag{9}$$

$$s = \hat{s} \quad \text{on } \partial B_{\text{S}} \tag{10}$$

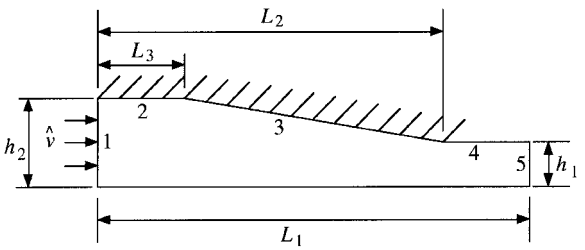

Figure 4. Round to round extrusion model.

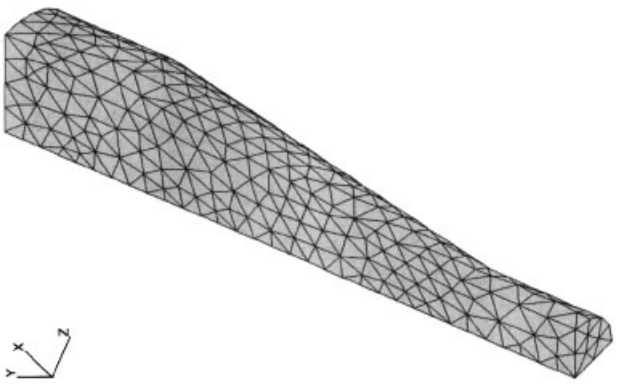

Figure 5. Mesh for round to round extrusion model.

where $\hat{\mathbf{v}}$ is the velocity specified on ∂B_{D}, $\hat{\mathbf{t}}$ is the traction specified on ∂B_{N}, $\mathbf{n}$ is the unit outward normal vector on ∂B and $\hat{s}$ is the state variable specified on ∂B_{S}. Furthermore, Equation (9) represents a simple, hydrodynamic friction law where ∂B_{F} is the part of the boundary with friction, η is the coefficient of hydrodynamic friction, $\mathbf{v}_{\mathrm{o}}$ is the tool velocity and $\mathbf{e}_{\mathrm{T}}$ is a unit vector tangent to the boundary. Boundary conditions (7)–(9) must be specified on the entire boundary for each degree of freedom (d.o.f.) without overlap, so $\partial B_{\mathrm{D}} \cup \partial B_{\mathrm{N}} \cup \partial B_{\mathrm{F}} = \partial B$ and $\partial B_a \cap \partial B_b = \emptyset$, for $a \neq b$, $a, b = \mathrm{D}, \mathrm{N}, \mathrm{F}$. The boundary condition on the state variable s, Equation (10), need only be specified on the entrance boundary where material is entering the domain (in a material reference frame, this is the initial condition).

3. STABILIZED FORMULATION

In the standard Galerkin procedure, Equation (1) is multiplied by an arbitrary weighting function $\mathbf{v}^*$ lying in the space V of kinematically admissible velocities and integrating by parts yields the usual weak form

$$\int_B \boldsymbol{\sigma}' : \mathbf{D}^* \, \mathrm{d}V - \int_B p \, \mathrm{div}\, \mathbf{v}^* \, \mathrm{d}V + \int_{\partial B_{\mathrm{F}}} \eta \mathbf{v} \cdot \mathbf{v}^* \, \mathrm{d}S = \mathbf{L}_{\mathrm{ext}}(\mathbf{v}^*) \tag{11}$$

Table II. Principal stresses comparison (unit: MPa).

Element type	Penalty (P2/P1)	Stabilized (P1/P1)	Penalty (P1/P1)
d.o.f	42578	2960	2960
$\sigma^{\mathrm{I}}_{\max}$	20.3	17.9	22.0
$\sigma^{\mathrm{I}}_{\min}$	−258.0	−263.0	−284.0
$\sigma^{\mathrm{II}}_{\max}$	14.4	6.35	15.4
$\sigma^{\mathrm{II}}_{\min}$	−264.0	−268.0	−293.0
$\sigma^{\mathrm{III}}_{\max}$	−2.72	−4.97	−5.03
$\sigma^{\mathrm{III}}_{\min}$	−273.0	−277.0	−301.0

where

$$\mathbf{L}_{\mathrm{ext}}(\mathbf{v}^*) = \int_{\partial B_{\mathrm{N}}} \hat{\mathbf{t}} \cdot \mathbf{v}^* \, \mathrm{d}S + \int_{\partial B_{\mathrm{F}}} \eta \mathbf{v}_{\mathrm{o}} \cdot \mathbf{v}^* \, \mathrm{d}S$$

The pressure field is indeterminate from kinematics due to incompressibility. The assumption of incompressible deformation defines a constraint equation (2) on the solution for the velocity field. Enforcing it in a weak sense through a weighting function p^* lying in the space P

$$\int_B (\operatorname{div} \mathbf{v}) p^* \, \mathrm{d}V = 0 \tag{12}$$

In addition, the state variable evolution equation assuming steady flow (5) provides the third governing Euler–Lagrange equation. Assuming a weighting function s^* lying in an admissible state variable space S yields

$$\int_B [\nabla s \cdot \mathbf{v} - g(\dot{\varepsilon}, s)] s^* \, \mathrm{d}V = 0 \tag{13}$$

Equations (11)–(13) are a three-field mixed formulation which can be put into matrix form by discretizing the domain and defining finite element interpolations for the velocity, pressure and state variable fields. The incompressibility constraint (12) is known to sometimes cause ill-conditioning which causes spurious pressure modes, and the convection equation (13) is also known to sometimes cause instabilities resulting in potentially large errors in the solution. The stabilized finite element method has been shown to be effective in handling both of these numerical instabilities [6] for linear problems. In this work, the same methodologies are applied to the non-linear problem defined above.

Stabilized finite element methods are generalized Galerkin methods where terms, which are functions of the Euler–Lagrange equations (in this paper, Equations (1), (2), and (5)), are added to enhance the stability of the method. A stabilization method to handle the ill-conditioning due to the incompressibility constraint has been presented in Reference [17] and will only be summarized here for completeness. The following Petrov–Galerkin formulation is defined

$$-\int_B (\operatorname{div} \boldsymbol{\sigma}) \cdot (\mathbf{v}^* + \delta \nabla p^*) \, \mathrm{d}V + \int_B (\operatorname{div} \mathbf{v}) p^* \, \mathrm{d}V = 0 \tag{14}$$

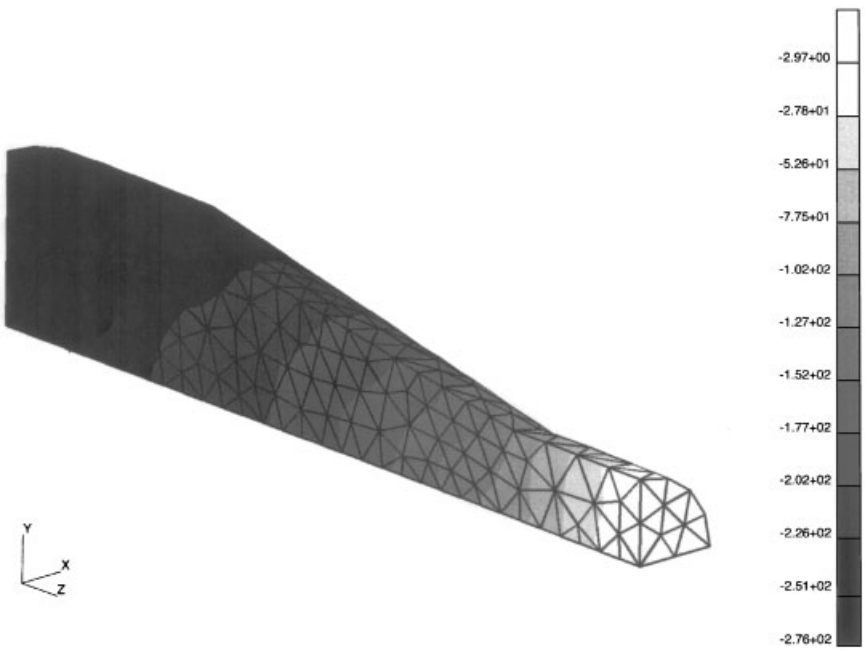

Figure 6. Stress σ_{zz} (MPa) with stabilization (P1/P1 elements).

where $\mathbf{v}^*$ in Equation (11) has been replaced by $\mathbf{v}^* + \delta\nabla p^*$ and the equation has not yet been integrated by parts. In addition, Equation (12) has been added. The parameter δ is a mesh-dependent stabilization parameter, which is chosen following Reference [14] as $\delta = \alpha h_e^2/2\mu$, where h_e is a characteristic element length for element e, α is a non-dimensional, non-negative, stability parameter and μ is as defined in Equation (6). Integrating the first term by parts, evaluating the stabilization term elementwise, and considering the arbitrariness of the weighting functions $\mathbf{v}^*$ and p^* results in the following system:

$$\int_B \boldsymbol{\sigma}' : \mathbf{D}^* \, \mathrm{d}V - \int_B p \, \mathrm{div}\, \mathbf{v}^* \, \mathrm{d}V + \int_{\partial B_F} \eta \mathbf{v} \cdot \mathbf{v}^* \, \mathrm{d}S = \mathbf{L}_{\mathrm{ext}}(\mathbf{v}^*) \tag{15}$$

$$\int_B (\mathrm{div}\, \mathbf{v}) p^* \, \mathrm{d}V + \sum_{e=1}^{n_{\mathrm{el}}} \int_{B_e} \frac{\alpha h_e^2}{2\mu} (\nabla p \cdot \nabla p^* - \mathrm{div}\, \boldsymbol{\sigma}' \cdot \nabla p^*) \, \mathrm{d}V = 0 \tag{16}$$

where Equation (15) is the same as Equation (11) and Equation (16) is same as Equation (12) with added stabilization terms.

Note in Equation (16), if linear elements are used to interpolate the velocity and the pressure fields, the second stabilization term involving the deviatoric stress is zero leaving only the first term. For higher order elements, this term, which depends in a complicated way on the gradient of the velocity field, must be computed. In this work, a local reconstruction method, following the work presented for 2D Navier–Stokes equations in Reference [19], is used. The reconstructed term is $\boldsymbol{\sigma}'$. The divergence of the reconstructed term can then be expressed

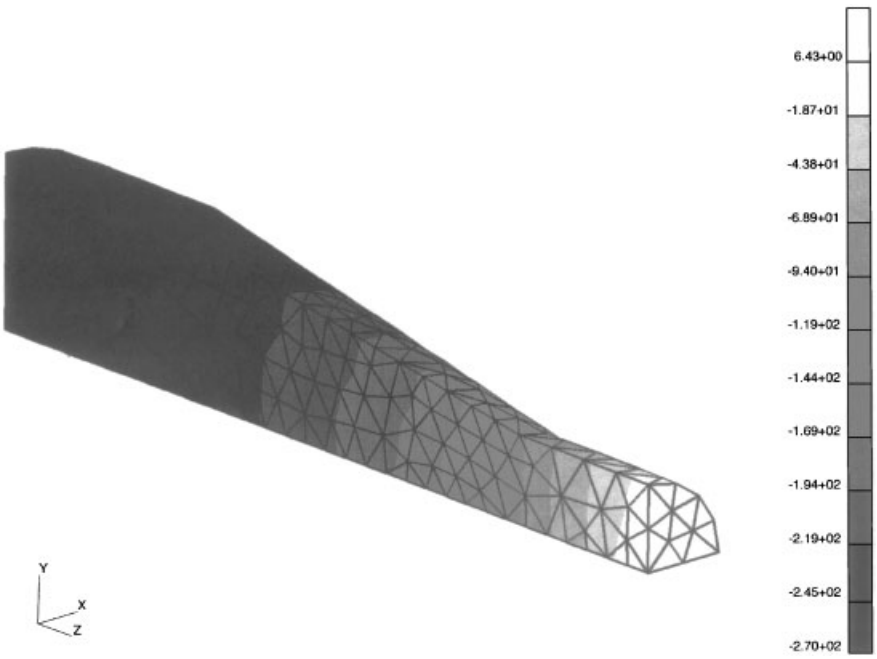

Figure 7. Pressure p (MPa) with stabilization (P1/P1 elements).

Table III. Principal stresses comparison (unit: MPa).

	Case (1)	Case (2)	Case (3)
$\sigma^{\mathrm{I}}_{\max}$	50.6	151.0	51.8
$\sigma^{\mathrm{I}}_{\min}$	−101.0	−158.0	−124.0
$\sigma^{\mathrm{II}}_{\max}$	30.8	130.0	30.8
$\sigma^{\mathrm{II}}_{\min}$	−104.0	−176.0	−130.0
$\sigma^{\mathrm{III}}_{\max}$	27.4	114.0	27.7
$\sigma^{\mathrm{III}}_{\min}$	−114.0	−188.0	−138.0

in terms of the element shape functions and the node quantities. This term is reconstructed to be a continuous variable, in a local sense, using an L_2 projection operator performed for each element. We write the stabilized term with the reconstructed divergence of the deviatoric stresses as

$$F(p^*) = \sum_{e=1}^{n_{\mathrm{el}}} \int_{B_e} \frac{\alpha h_e^2}{2\mu} \operatorname{div} \boldsymbol{\sigma}' \cdot \nabla p^* \, \mathrm{d}V \tag{17}$$

In a similar fashion, the convection equation resulting from the state variable evolution equation will be stabilized using a Petrov–Galerkin-type formulation. Specifically, the weighting

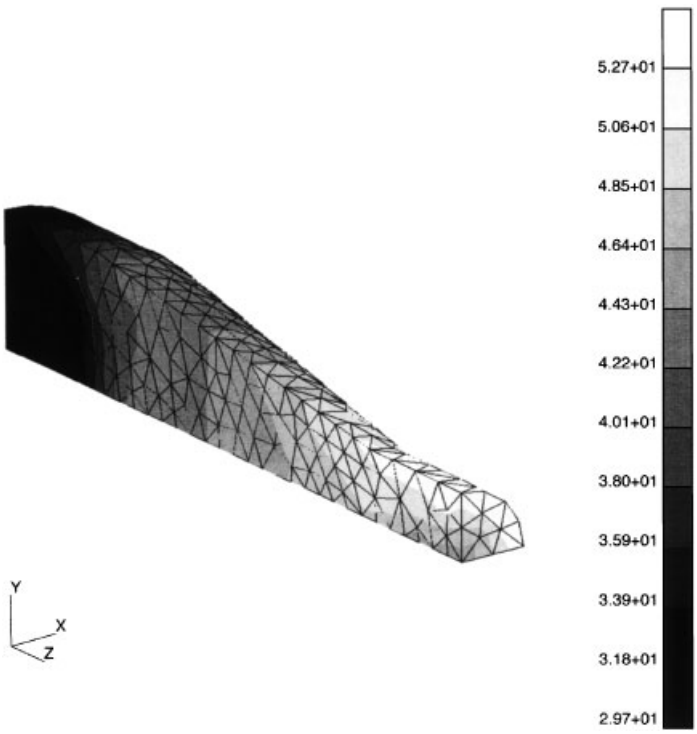

Figure 8. State variable s (MPa) with stabilization (P1/P1 elements).

function s^* in Equation (13) will be replaced by the following perturbed weighting function:

$$q^* = s^* + \tau_e \nabla s^* \cdot \mathbf{v} \tag{18}$$

The parameter τ_e is chosen to be $\tau_e = \beta h_e / 2|\mathbf{v}|$ following Reference [18], where β is a non-dimensional, non-negative stability parameter similar to α in Equation (16). Thus, the following form for the state variable evolution results

$$\int_B [\nabla s \cdot \mathbf{v} - g(\dot{\varepsilon}, s)](s^* + \tau_e \nabla s^* \cdot \mathbf{v}) \, \mathrm{d}V = 0 \tag{19}$$

The stabilization term in Equation (19) is evaluated elementwise resulting finally in

$$\int_B [\nabla s \cdot \mathbf{v} - g(\dot{\bar{\varepsilon}}, s)] s^* \, \mathrm{d}V + \sum_{e=1}^{n_{\mathrm{el}}} \int_{B_e} \frac{\beta h_e}{2|\mathbf{v}|} [\nabla s \cdot \mathbf{v} - g(\dot{\varepsilon}, s)](\mathbf{v} \cdot \nabla s^*) \, \mathrm{d}V = 0 \tag{20}$$

Note that the stabilization term is a function of the Euler–Lagrange Equation (5), and thus a solution to Equation (20) will be consistent.

So now the resulting stabilized problem is to find $(\mathbf{v}, p, s)$ lying in the space $V \times P \times S$ that satisfies Equations (15), (16) and (20). A Newton–Raphson procedure will be used to solve the non-linear system, and the required linearized formulation follows.

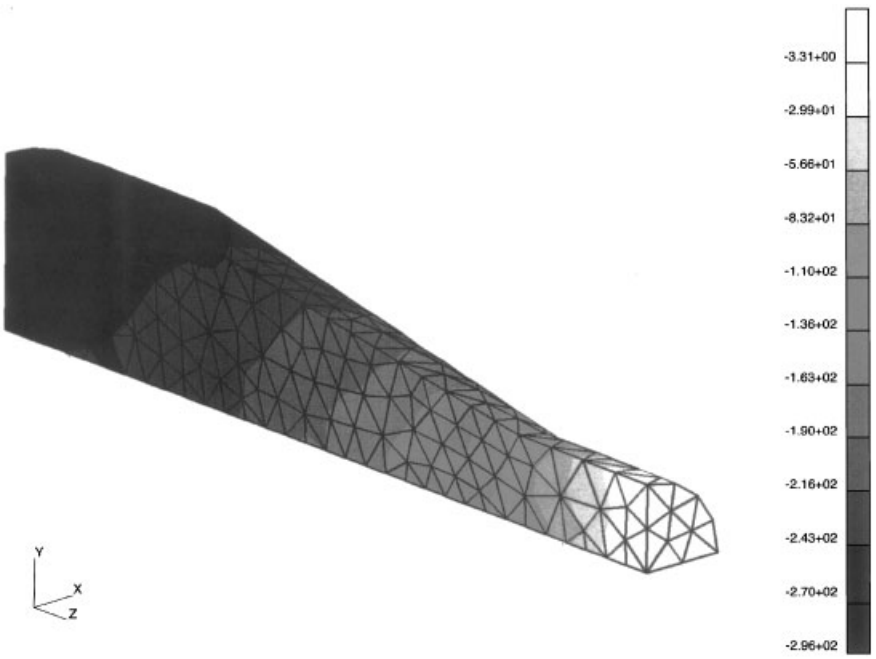

Figure 9. Stress σ_{zz} (MPa) without stabilization (penalty P1/P1 elements).

4. LINEARIZATION

First, we represent Equations (15), (16) and (20) in a short form as

$$\begin{aligned} G_{(\mathbf{v},p,s)}(\mathbf{v}^*) &= \mathbf{L}_{\text{ext}}(\mathbf{v}^*) \\ R_{(\mathbf{v},p,s)}(p^*) &= F(p^*) \\ T_{(\mathbf{v},s)}(s^*) &= 0 \end{aligned} \tag{21}$$

where

$$G_{(\mathbf{v},p,s)}(\mathbf{v}^*) = \int_B \boldsymbol{\sigma}' : \mathbf{D}^* \, \mathrm{d}V - \int_B p \operatorname{div} \mathbf{v}^* \, \mathrm{d}V + \int_{\partial B_{\mathrm{F}}} \eta \mathbf{v} \cdot \mathbf{v}^* \, \mathrm{d}S$$

$$R_{(\mathbf{v},p,s)}(p^*) = \int_B (\operatorname{div} \mathbf{v}) p^* \, \mathrm{d}V + \sum_{e=1}^{n_{\text{el}}} \int_{B^e} \frac{\alpha h_e^2}{2\mu} (\nabla p \cdot \nabla p^*) \, \mathrm{d}V$$

$$T_{(\mathbf{v},s)}(s^*) = \int_B [\nabla s \cdot \mathbf{v} - g(\dot{\varepsilon}, s)] s^* \, \mathrm{d}V + \sum_{e=1}^{n_{\text{el}}} \int_{B_e} \frac{\beta h_e}{2|\mathbf{v}|} [\nabla s \cdot \mathbf{v} - g(\dot{\varepsilon}, s)](\mathbf{v} \cdot \nabla s^*) \, \mathrm{d}V$$

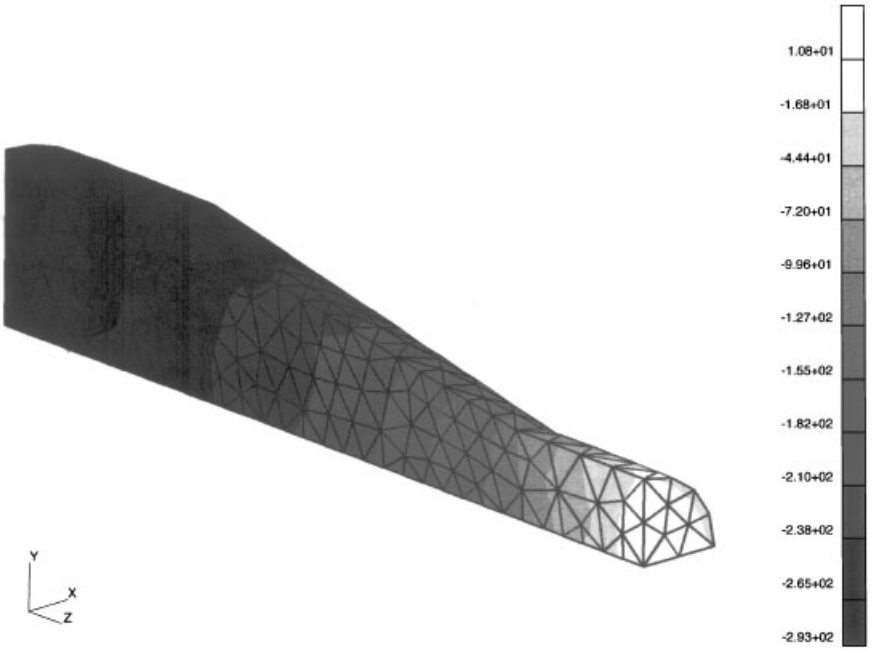

Figure 10. Pressure p (MPa) without stabilization (penalty P1/P1 elements).

Linearization of Equation (21) leads to the following system of equations:

$$\begin{aligned} a_{(\mathbf{v},s)}(\Delta\mathbf{v},\mathbf{v}^*)+b(\Delta p,\mathbf{v}^*)+h_{(\mathbf{v},s)}(\Delta s,\mathbf{v}^*) &= \mathbf{L}_{\text{ext}}(\mathbf{v}^*)-G_{(\mathbf{v},p,s)}(\mathbf{v}^*) \\ c_{(\mathbf{v},s)}(\Delta\mathbf{v},p^*)+c_{\text{stab}(\mathbf{v},p,s)}(\Delta\mathbf{v},p^*)+m_{\text{stab}(\mathbf{v},s)}(\Delta p,p^*)+k_{\text{stab}(\mathbf{v},p,s)}(\Delta s,p^*) &= F(p^*)-R_{(\mathbf{v},p)}(\mathbf{p}^*) \\ d_{(\mathbf{v},s)}(\Delta\mathbf{v},s^*)+d_{\text{stab}(\mathbf{v},s)}(\Delta\mathbf{v},s^*)+e_{(\mathbf{v},s)}(\Delta s,s^*)+e_{\text{stab}(\mathbf{v},s)}(\Delta s,s^*) &= -T_{(\mathbf{v},s)}(s^*) \end{aligned} \tag{22}$$

where

$$a_{(\mathbf{v},s)}(\Delta\mathbf{v},\mathbf{v}^*)=\int_B\left\{\frac{4}{9\dot{\varepsilon}^2}\left[\frac{\partial f(\dot{\varepsilon},s)}{\partial\dot{\varepsilon}}-\frac{f(\dot{\varepsilon},s)}{\dot{\varepsilon}}\right][\mathbf{D}:\nabla(\Delta\mathbf{v})]\mathbf{D}+\frac{2f(\dot{\varepsilon},s)}{3\dot{\varepsilon}}\Delta\mathbf{D}\right\}:\mathbf{D}^*\,\mathrm{d}V$$

$$+\int_{\partial B_F}\eta\Delta\mathbf{v}\cdot\mathbf{v}^*\,\mathrm{d}S$$

$$b(\Delta p,\mathbf{v}^*)=-\int_B\Delta p\,\mathrm{div}\,\mathbf{v}^*\,\mathrm{d}V$$

$$h_{(\mathbf{v},s)}(\Delta s,\mathbf{v}^*)=\int_B\frac{2}{3\dot{\varepsilon}}\frac{\partial f(\dot{\varepsilon},s)}{\partial s}\Delta s\mathbf{D}:\mathbf{D}^*\,\mathrm{d}V$$

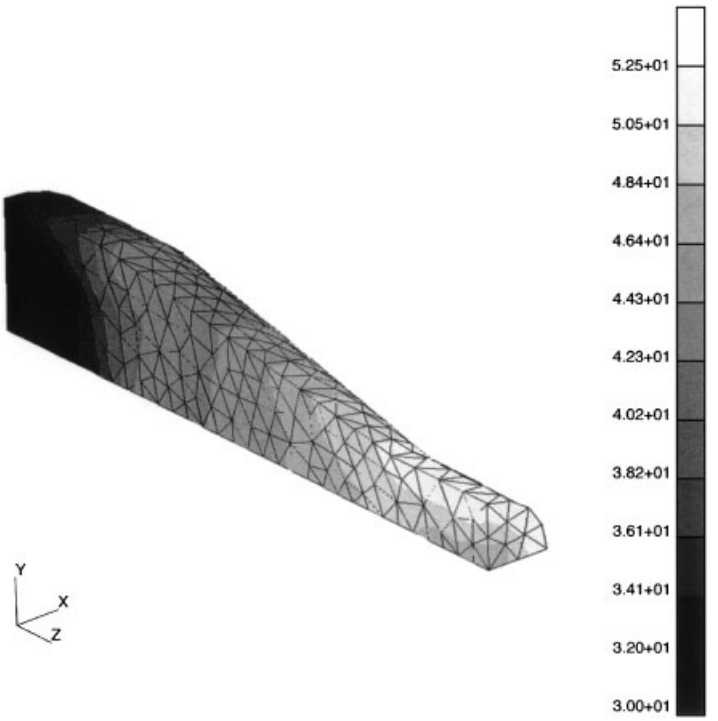

Figure 11. State variable s (MPa) without stabilization (penalty P1/P1 elements).

$$c_{(\mathbf{v},s)}(\Delta\mathbf{v},\, p^*) = \int_B \operatorname{div}\Delta\mathbf{v}\, p^*\, \mathrm{d}V$$

$$c_{\mathrm{stab}(\mathbf{v},\,p,s)}(\Delta\mathbf{v},\, p^*) = -\sum_{e=1}^{n_{\mathrm{el}}} \int_B \frac{\alpha h_e^2}{9\mu^2\dot{\varepsilon}^2}\left[\frac{\partial f(\dot{\varepsilon},s)}{\partial\dot{\varepsilon}} - \frac{f(\dot{\varepsilon},s)}{\dot{\varepsilon}}\right][\mathbf{D}:\nabla(\Delta\mathbf{v})](\nabla p\cdot\nabla p^*)\,\mathrm{d}V$$

$$m_{\mathrm{stab}(\mathbf{v},s)}(\Delta p,\, p^*) = \sum_{e=1}^{n_{\mathrm{el}}} \int_{B^e} \frac{\alpha h_e^2}{2\mu}[\nabla(\Delta p)\cdot\nabla p^*]\,\mathrm{d}V$$

$$k_{\mathrm{stab}(\mathbf{v},\,p,s)}(\Delta s,\, p^*) = -\sum_{e=1}^{n_{\mathrm{el}}} \int_{B^e} \frac{\alpha h_e^2}{6\mu^2\dot{\varepsilon}}\frac{\partial f(\dot{\varepsilon},s)}{\partial s}\Delta s(\nabla p\cdot\nabla p^*)\,\mathrm{d}V$$

$$d_{(\mathbf{v},s)}(\Delta\mathbf{v},s^*) = \int_B \left[\nabla s\cdot\Delta\mathbf{v} - \frac{2}{3\dot{\varepsilon}}\frac{\partial g(\dot{\varepsilon},s)}{\partial\dot{\varepsilon}}\,\mathbf{D}\cdot\nabla(\Delta\mathbf{v})\right] s^*\,\mathrm{d}V$$

$$d_{\mathrm{stab}(\mathbf{v},s)}(\Delta\mathbf{v},s^*) = \sum_{e=1}^{n_{\mathrm{el}}} \int_{B_e} \frac{\beta h_e}{2|\mathbf{v}|}\left\{\left[\nabla s\cdot\Delta\mathbf{v} - \frac{2}{3}\frac{\partial g(\dot{\varepsilon},s)}{\partial\dot{\varepsilon}}\frac{1}{\dot{\varepsilon}}\,\mathbf{D}\cdot\nabla(\Delta\mathbf{v})\right](\mathbf{v}\cdot\nabla s^*)\right.$$
$$\left. + (\nabla s\cdot\mathbf{v} - g(\dot{\varepsilon},s))(\Delta\mathbf{v}\cdot\nabla s^*) - \frac{1}{|\mathbf{v}|^2}(\nabla s\cdot\mathbf{v} - g(\dot{\varepsilon},s))(\mathbf{v}\cdot\Delta\mathbf{v})(\mathbf{v}\cdot\nabla s^*)\right\}\mathrm{d}V$$

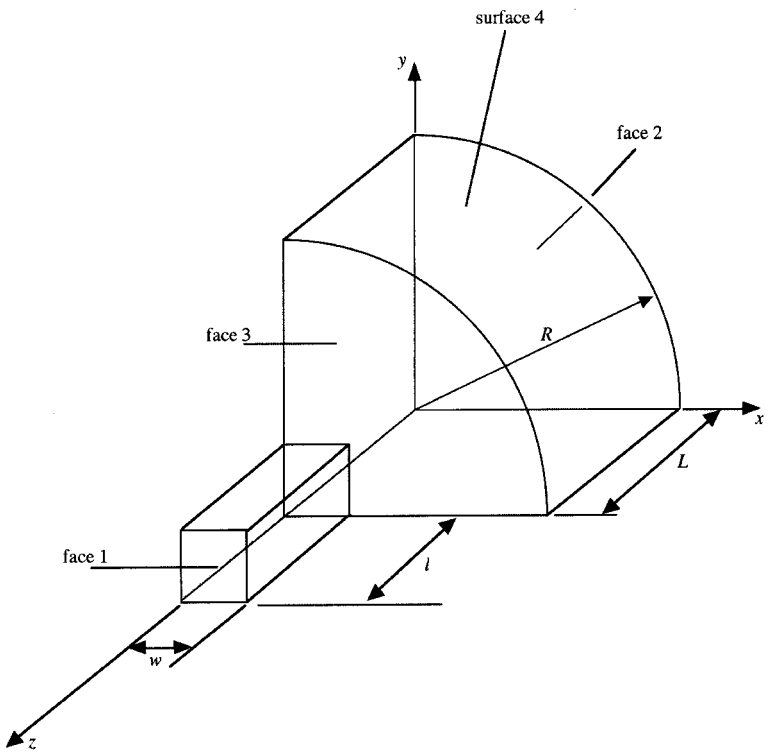

Figure 12. Round to square extrusion model.

$$e_{(\mathbf{v},s)}(\Delta s, s^*) = \int_{B_e} \left[\nabla(\Delta s) \cdot \mathbf{v} - \frac{\partial g(\dot{\varepsilon}, s)}{\partial s} \Delta s \right] s^* \, \mathrm{d}V$$

$$e_{\mathrm{stab}(\mathbf{v},s)}(\Delta s, s^*) = \sum_{e=1}^{n_{\mathrm{el}}} \int_B \frac{\beta h_e}{2|\mathbf{v}|} \left[\nabla(\Delta s) \cdot \mathbf{v} - \frac{\partial g(\dot{\varepsilon}, s)}{\partial s} \Delta s \right] (\mathbf{v} \cdot \nabla s^*) \, \mathrm{d}V$$

All that remains is to define the constitutive functions f and g.

5. CONSTITUTIVE LAW AND PROGRESSIVE SOLUTION APPROACH

The constitutive laws considered herein are a simple power law, which is selected because an analytic solution can be determined for comparison in the first example, and the model presented in Reference [20]. For the case of the power law, the function f is taken to be

$$f_{\mathrm{power}} = s \left(\frac{\dot{\varepsilon}}{c} \right)^m \tag{23}$$

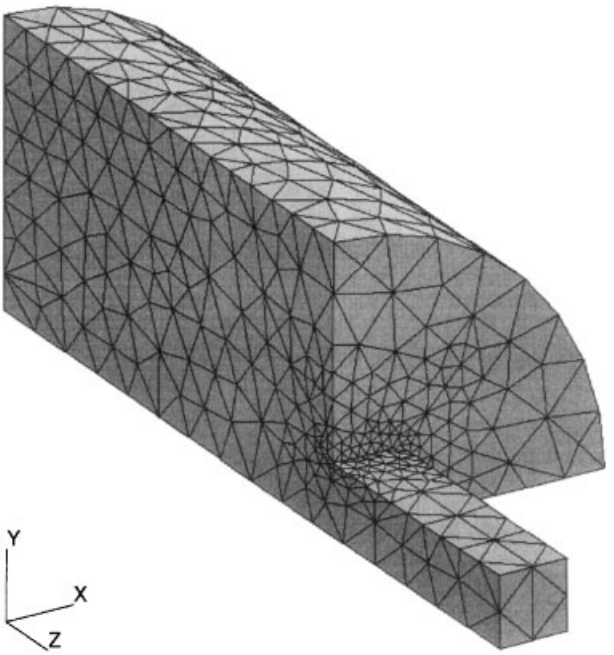

Figure 13. Mesh of round to square extrusion model.

where $c = 1.0\ \mathrm{s}^{-1}$, and $m = 0.05$. The function f for the model presented in Reference [20] can be expressed as

$$f_{\mathrm{BKA}} = \frac{s}{\xi}\ \sinh^{-1}\left(\frac{\dot{\varepsilon}}{\bar{A}}\right)^{m} \tag{24}$$

where $\bar{A} = A\exp(-Q/R\theta)$, R is the ideal gas constant, Q is the thermal activation energy, θ is the absolute temperature and A, ξ and m are the material parameters. For 1100 aluminum at 450°C, the parameters for Equation (24) are $\bar{A} = 4.13 \times 10^{-6}\ \mathrm{s}^{-1}$, $\xi = 7.00$, $m = 0.23348$. For both models, the state variable evolution equation, defined by function g, is taken to be the one given in Reference [20]

$$\begin{aligned} \dot{s} &= g(\dot{\varepsilon}, s) = \left[h_0 \left|1 - \frac{s}{\bar{s}}\right|^{a} \operatorname{sign}\left(1 - \frac{s}{\bar{s}}\right)\right] \dot{\varepsilon} \\ \bar{s} &= \tilde{s}\left(\frac{\dot{\varepsilon}}{\bar{A}}\right)^{n} \end{aligned} \tag{25}$$

where $h_0 = 1115.6$ MPa, $a = 1.3$, $\tilde{s} = 18.9$ MPa, and $n = 0.07049$.

An issue related to the constitutive law and the numerics is convergence of the Newton–Raphson iteration. Because the constitutive laws, specifically, Equations (23) and (24), considered herein are highly non-linear, obtaining a trial solution within the radius of convergence is problematic [21]. In Reference [17], a simple strategy is presented whereby the system

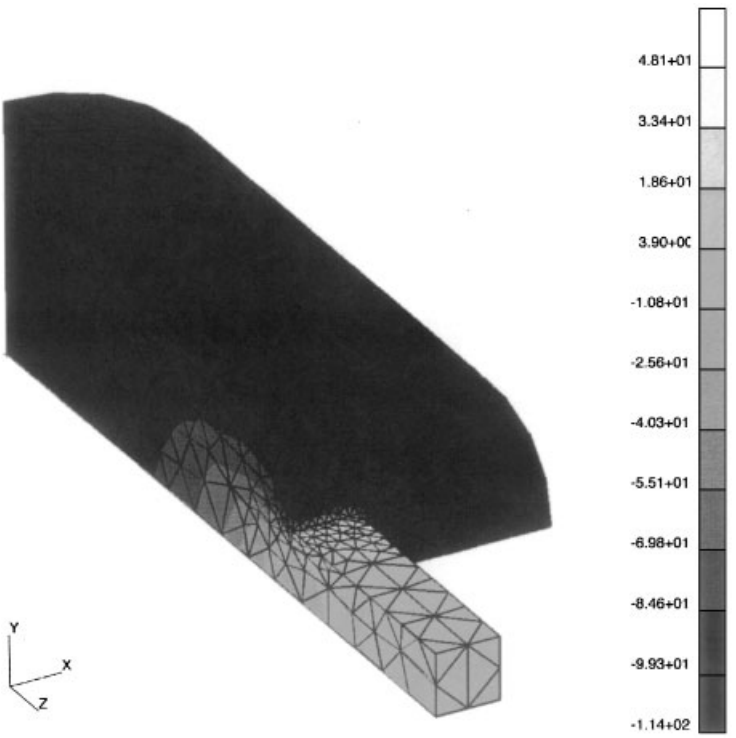

Figure 14. Stress σ_{zz} (MPa) with stabilization(P1/P1 elements).

equations are made progressively more non-linear in a stepwise manner, and the solution from the previous step is used as the trial solution in the next step. In this method, the trial solution at each step is within the radius of convergence allowing for rapid convergence with the Newton–Raphson algorithm. An automatic stepping procedure, similar to an automatic time-stepping procedure, is used in order to optimize the step size. This same procedure is used in the examples presented herein. Specifically, the following modified forms of Equations (23) and (24) are used:

$$f_1(t) = s\left(\frac{\dot{\varepsilon}}{c}\right)^{(m/t)} \tag{26}$$

$$f_2(t) = (1-t)\mathrm{e}^{-t}\hat{s}\dot{\varepsilon} + (1-(1-t)\mathrm{e}^{-t})f_{\mathrm{BKA}} \tag{27}$$

where in Equation (26), $m \leqslant t \leqslant 1$, and in Equation (27), $0 \leqslant t \leqslant 1$. Thus, when t is at its lower limit, the equation becomes linear, and when t is at its upper limit, the fully non-linear equation is recovered. The parameter t is then varied from the lower limit to the upper limit progressing from linear to fully non-linear behaviour. The parameter $\hat{s}$ is the initial value of s prescribed in ∂B_s and is taken to be 29.5 MPa in the following examples.

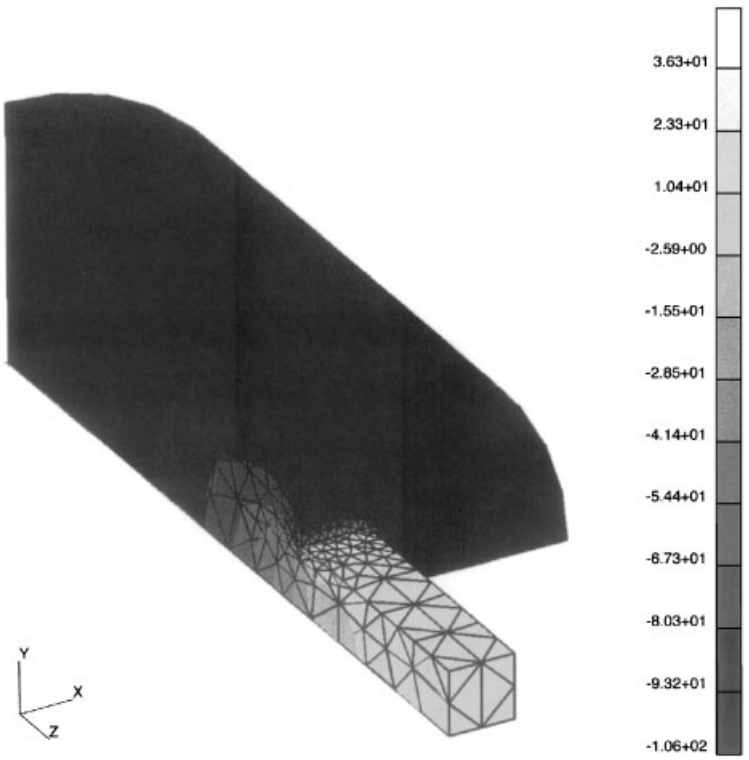

Figure 15. Pressure p (MPa) with stabilization (P1/P1 elements).

6. NUMERICAL EXAMPLES

The above stabilized formulation has been implemented into an object-oriented finite element framework, named Trellis, developed in the Scientific Computation Research Center at Rensselaer Polytechnic Institute [22]. Hierarchic shape functions are used. In order to provide a quantitative assessment of the formulations, three examples are investigated: radial flow in a cylinder, from which we can compare the finite element results with the analytical solution, and two extrusion problems, which will demonstrate more practical applications of this formulation. The system relative convergence tolerance for the Newton–Raphson solver is taken to be 1.e-6 for the first example and 1.e-5 for the remaining examples.

6.1. Hollow cylinder with radial viscoplastic flow

Figure 1 shows the geometry in this example involving radial plastic flow in a hollow cylinder. Radial velocities are specified on the inner radius. The hollow cylinder has inner radius $R_1 = 1$ m and outer radius $R_2 = 2$ m. Owing to symmetry, only one quarter of the model is considered. For the finite element analysis, 2445 tetrahedral elements are used (see Figure 2). The velocity, pressure and the state variable are interpolated with equal order

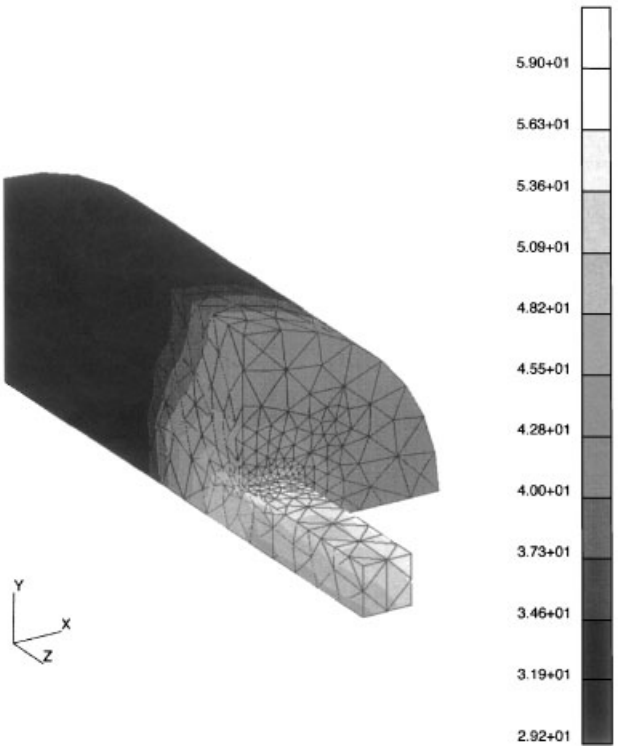

Figure 16. State variable s (MPa) with stabilization (P1/P1 elements).

hierarchic shape functions. The solution is sought by applying a non-zero radial velocity and an initial state variable boundary condition on the inner radius ($\hat{v} = 0.1\,\mathrm{m\,s^{-1}}$ and $\hat{s} = 29.5\,\mathrm{MPa}$ on $r = R_1 = 1\,\mathrm{m}$). The power law model (23) is employed in this example. In order to verify the computational accuracy of the stabilized finite element formulation, we test a group of stabilization parameters $\alpha = 10^{-6}, 10^{-5}, 10^{-4}, 10^{-3}, 10^{-2}, 10^{-1}$ and 1.0. The stabilization parameter β is fixed at $\beta = 1.0$ because this has been shown to be optimal for problems involving pure convection (see, for example, Reference [23]) as is the case here in Equation (5). For this particular cylindrical steady-state flow problem, the analytical solution for velocity and stress fields is

$$\begin{aligned} v_r &= R_1 \frac{\hat{v}}{r}, \quad \sigma'_{rr} = -\frac{\bar{\sigma}}{\sqrt{3}}, \quad \sigma'_{\theta\theta} = \frac{\bar{\sigma}}{\sqrt{3}}, \quad \bar{\sigma} = s\left[\frac{2}{\sqrt{3}} R_1 \frac{\hat{v}}{r^2}\right]^m \\ p &= -\left(1 - \frac{1}{m}\right)\frac{\bar{\sigma}}{\sqrt{3}} - \frac{1}{\sqrt{3}m}\bar{\sigma}_{R_2} \\ \sigma_{rr} &= \frac{1}{\sqrt{3}m}(\bar{\sigma}_{R_2} - \bar{\sigma}) \\ \sigma_{\theta\theta} &= \left(2 - \frac{1}{m}\right)\frac{\bar{\sigma}}{\sqrt{3}} + \frac{1}{(\sqrt{3}m)}\bar{\sigma}_{R_2} \end{aligned} \tag{28}$$

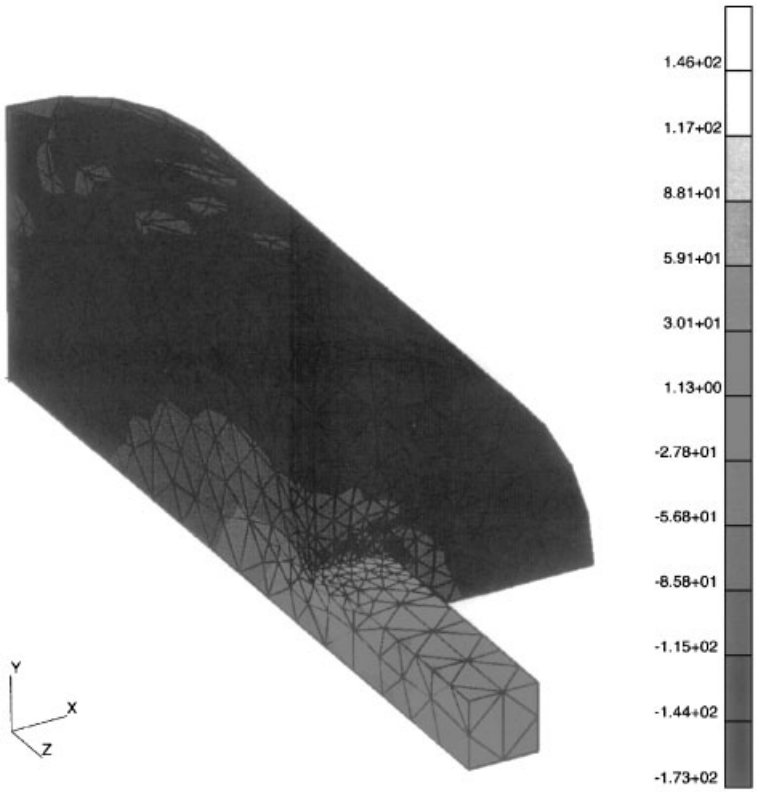

Figure 17. Stress σ_{zz} (MPa) without stabilization (penalty P1/P1 elements).

where $\bar{\sigma}_{R_2}$ is $\bar{\sigma}$ evaluated at $r = R_2$. For the state variable field s, combining Equation (25) with Equation (5) and using the known velocity field in Equation (28) yields the following ordinary differential equation:

$$\begin{aligned} \frac{\mathrm{d}s}{\mathrm{d}r} &= \frac{2}{\sqrt{3}} \frac{h_0}{r} \left| 1 - \frac{s}{\bar{s}} \right|^a \operatorname{sign}\left(1 - \frac{s}{\bar{s}}\right) \\ s|_{r=R_1} &= \hat{s} \end{aligned} \tag{29}$$

which can be solved accurately using the fourth-order Runge–Kutta method.

A discrete sum norm error ($\mathscr{SNE}$) is defined to compare the resulting pressure and state variable fields from the stabilized mixed finite element method (SFEM) with the above analytical solution. The $\mathscr{SNE}$ for the pressure is defined as

$$\mathscr{SNE} = \frac{1}{\hat{s}} \sqrt{\frac{1}{K_{\text{int}}} \sum_{\text{int}=1}^{K_{\text{int}}} [p^{(\text{int})} - p^{A(\text{int})}]^2} \tag{30}$$

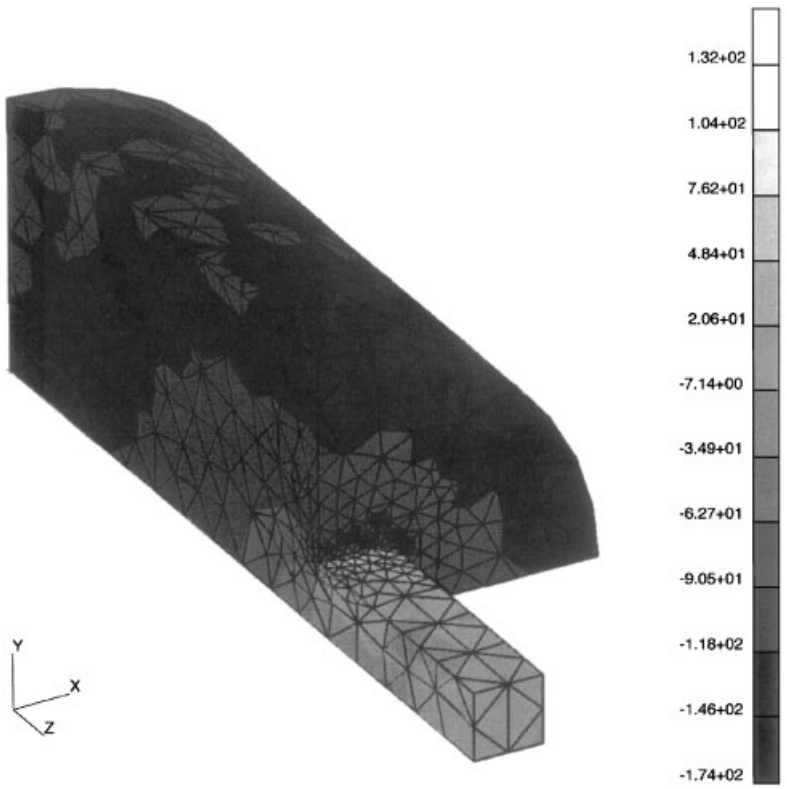

Figure 18. Pressure p (MPa) without stabilization (penalty P1/P1 elements).

where K_{int} is the total number of integration points in the whole domain, $p^{(\text{int})}$ is the pressure obtained at integration point *int* by the SFEM, and $p^{A(\text{int})}$ is the analytically determined pressure at the same point, see Equation (28). A similar relation is defined for the state variable: however, the comparison is with the solution to Equation (29) found using a fourth-order Runge–Kutta algorithm.

The results for this example are shown in Figure 3 and Table I. Figure 3 shows the $\mathscr{SNE}$ results of the pressure and state variable for different stabilization parameters α and $\beta = 1.0$. From the figure we can see that the $\mathscr{SNE}$ for quadratic elements is much smaller than that of the linear elements, as expected, and they have minimum error at differing values of α. For quadratic elements, the lowest $\mathscr{SNE}$ is at $\alpha = 10^{-1}$ for the pressure and at $\alpha = 10^{-2}$ for the state variable field. For linear elements, the lowest $\mathscr{SNE}$ is at $\alpha = 0.1$ for both the pressure and state variable fields. It was also found that for different meshes, these optimal values for α remained unchanged. Table I gives, at some positions along the radial direction, a comparison of the radial velocity between the exact (to within round-off error) solution and the SFEM solution where linear interpolation functions are used for the velocity, pressure and state variable fields. The results are in good agreement with the maximum relative error no larger than 0.38%. Finally, it should also be noted that a converged solution could not be obtained when $\alpha = 0$.

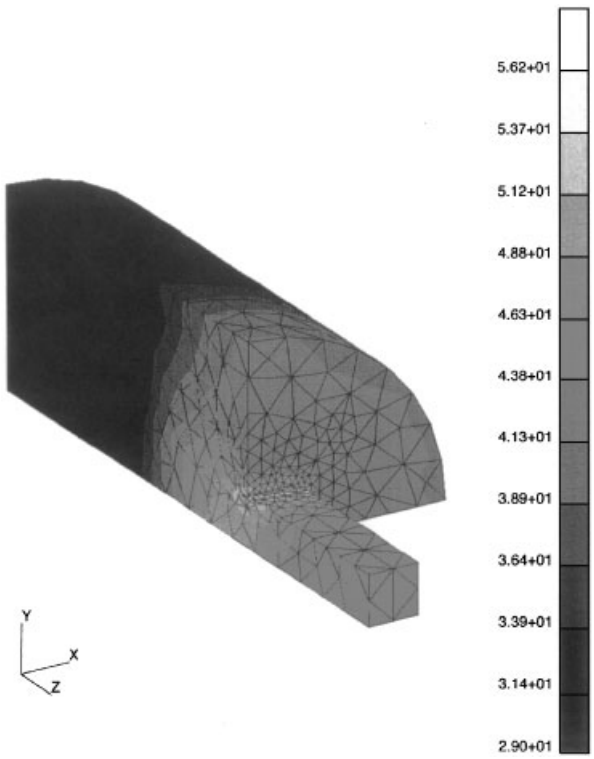

Figure 19. State variable s (MPa) without stabilization (penalty P1/P1 elements).

6.2. *Metal extrusion: round to round*

Axisymmetric metal extrusion is considered. Figure 4 gives the geometry and boundary conditions for the extrusion problem. The bottom line is the centerline. Faces 2 and 3 are assumed to be in frictional contact with the die or container. The geometric parameters are: $L_1 = 0.05\,\text{m}$, $L_2 = 0.04\,\text{m}$, $L_3 = 0.01\,\text{m}$, $h_1 = 0.005\,\text{m}$, $h_2 = 0.01\,\text{m}$. Although the problem is an axisymmetric problem, it is discretized in three dimensions. One-quarter of the model is considered due to the symmetry. The model is discretized into 2201 tetrahedral linear elements (see Figure 5) in which the velocity, pressure, and state variable fields are interpolated with hierarchic shape functions. The velocity is applied at the entrance (face 1). The value of the extrusion velocity on the entrance is $v = \hat{v} = 0.01\,\text{m}\,\text{s}^{-1}$. The material relation employed in this example is the model presented in Reference [20], Equation (24).

The stabilization parameter α is chosen based on the result of example 1. Thus, since linear elements are used in this example, $\alpha = 0.1$, and the stabilized parameter for the state variable evolution is $\beta = 1.0$. The coefficient of friction η is taken to be $1000\,\text{MPa}\,\text{s}\,\text{m}^{-1}$.

The results are shown in Table II and Figures 6–11. For comparison, the analysis was also performed using a penalty method with $\alpha = 0$, i.e. without stabilization for handling the incompressibility, and with P1/P1 and P2/P1 elements. For clarification, P1/P1 means linear velocity, pressure and state variable interpolation and P2/P1 means quadratic velocity and

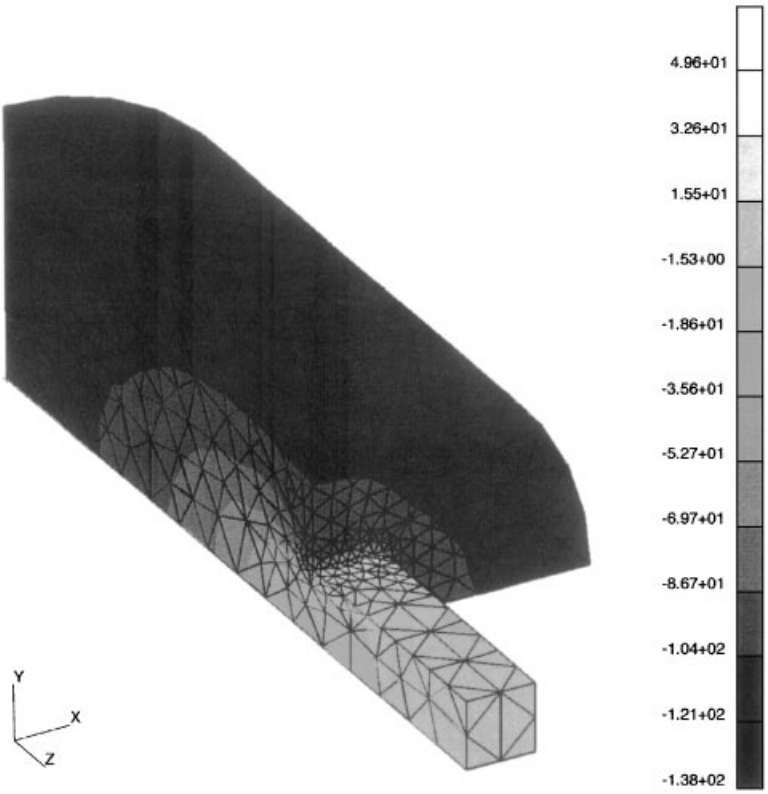

Figure 20. Stress σ_{zz} (MPa) with friction and stabilization (P1/P1 elements).

linear pressure and state variable interpolation. The number of d.o.f. that must be solved for, given a fixed mesh, is also listed for each element type in Table II. The penalty parameter used for imposing the incompressibility for the cases where $\alpha = 0$ was taken to be $\mu \times 10^7$, where μ is as defined in Equation (6). The integrand of Equation (12) is multiplied by the penalty parameter and the equation is then added to Equation (11). Table II shows a comparison of the principal stresses. Since the P2/P1 element is inherently stable and is higher order in the velocity field, it is expected to give the most accurate results. The stabilized results for the P1/P1 element compare favorably to the higher order, stable, P2/P1 element, but require solving for an order of magnitude fewer d.o.f. The P1/P1 element without stabilization for handling the incompressibility condition gives relatively poor results. Figures 6–8 show the σ_{zz} component of the stress, pressure and state variable fields with stabilization. Figures 9–11 show the σ_{zz} component of the stress, pressure and state variable fields without stabilization. The oscillations in the stress σ_{zz} are evident for the case with the P1/P1 element without stabilization. It should be noted that the σ_{zz} component of the stress is chosen to be shown because it is along the extrusion direction, and because it includes the pressure contribution which is where the oscillations are typically a problem. Deviatoric stresses and the von Mises stress are not shown because they are not strongly affected by instabilities resulting from nearly incompressible behaviour.

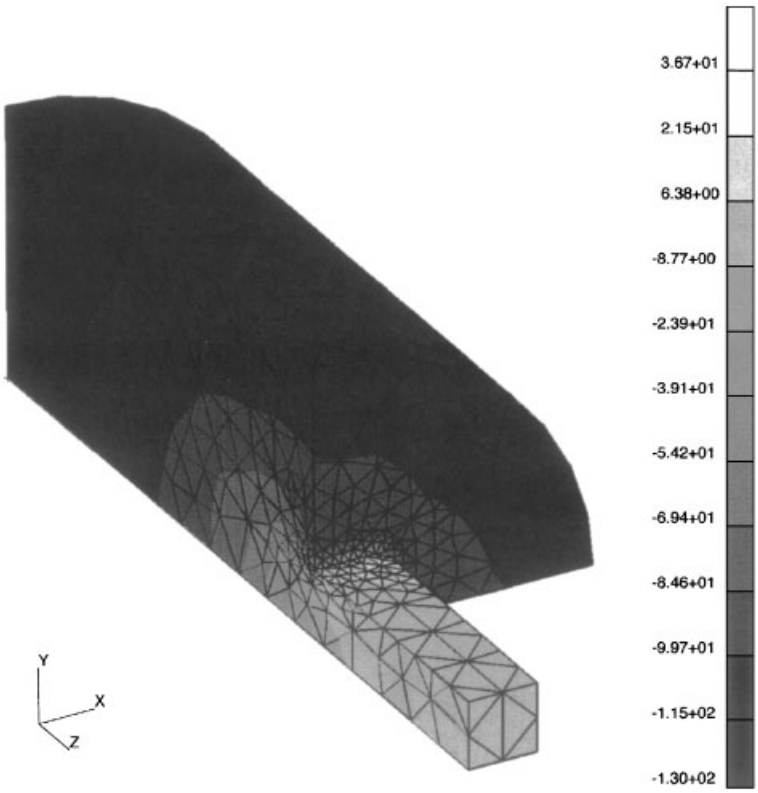

Figure 21. Pressure p (MPa) with friction and stabilization (P1/P1 elements).

6.3. *Metal extrusion: round to square*

A round to square three-dimensional extrusion problem is investigated. Figure 12 gives the geometry. Owing to the symmetry, only one-quarter of the model is considered. The geometric parameters are: $L = 2.0$ m, $l = 1.0$ m, $R = 1.0$ m, $w = 0.25$ m. The model is discretized into 5817 tetrahedral elements (see Figure 13) in which a fine mesh is made around the exit. The velocity, pressure and state variable interpolation functions are taken to be linear in each case. The extrusion velocity is applied at the entrance (face 2). The value of extrusion velocity is $v = \hat{v} = 0.1$ m/s^{-1}. The workpiece is assumed to be in frictional contact with the die and container (face 3 and surface 4). The material relation employed in this example is again the model presented in Reference [20], Equation (24).

The stabilized parameter α can be chosen based on the result of example 6.1; thus, the stabilization parameters are selected to be $\alpha = 0.1$ and $\beta = 1.0$. The following cases are considered for this example:

(1) No friction, with stabilization, i.e. $\eta = 0.0$, $\alpha = 0.1$ and $\beta = 1$.
(2) No friction, no stabilization, i.e. $\eta = 0.0$, $\alpha = 0.0$ and $\beta = 0.0$.
(3) With both friction and stabilization, i.e. $\eta = 100.0$ MPa s^{-1} m^{-1}, $\alpha = 0.1$ and $\beta = 1$.

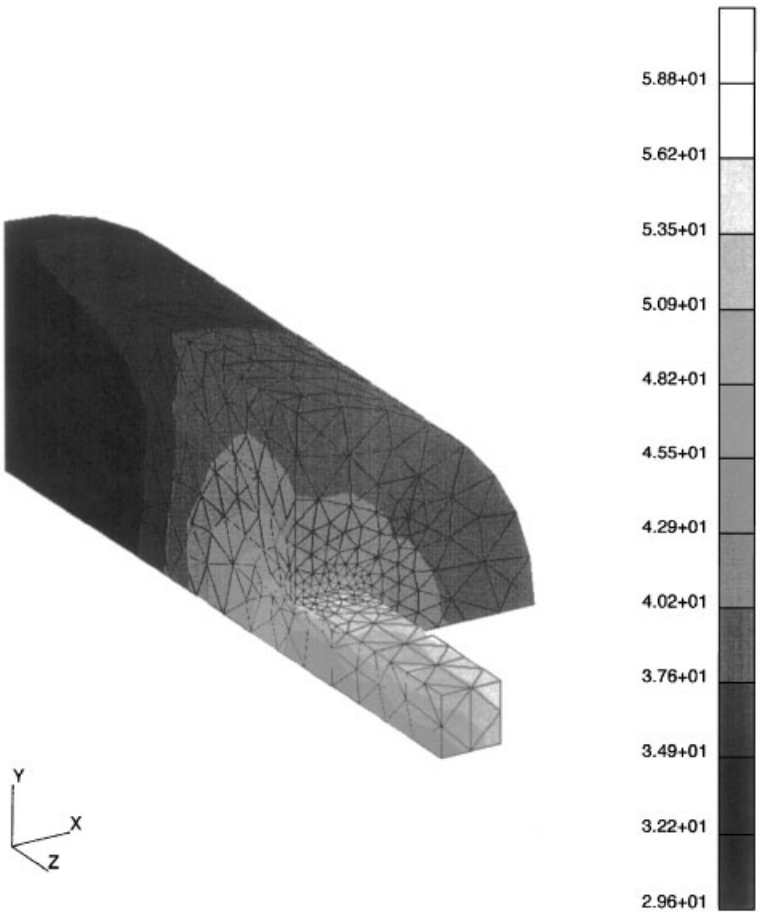

Figure 22. State variable s (MPa) with friction and stabilization (P1/P1 elements).

The results are shown in Table III and Figures 14–22. Table III shows a comparison of the principal stresses. Figures 14–16 show the σ_{zz} component of the stress, pressure and state variable fields for case (1), i.e. with stabilization and without friction. Figures 17–19 show the σ_{zz} component of the stress, pressure and state variable fields for case (2), i.e. without both stabilization and friction. The results without stabilization show oscillations in the stress and pressure fields, which can also be seen in the range of the principal stresses (see Table III). Figures 20–22 gives the results for stress, pressure and state variable fields in case (3) with both friction and stabilization.

7. CONCLUSIONS

This paper presents a three-field (velocity, pressure, and state variable), stabilized, mixed finite element formulation for modelling metal-forming problems. The formulation considers

the standard mixed finite element equations for viscoplastic flow with a convection-type state variable equation. The incompressibility condition and the convection equation associated with the state variable evolution are sometimes sources of instability. Two mesh-dependent stabilization terms, associated with the pressure and state variable fields, are added to the usual Galerkin formulation. These terms are functions of the residual of the Euler–Lagrange equations and are added elementwise to enhance the stability of the three-field mixed finite element formulation. Linearization of the weak form is derived to enable a Newton–Raphson implementation into an object-oriented finite element framework. A progressive solution strategy is used for improving convergence.

Numerical examples using very non-linear material constitutive laws, typical for metals, are presented in this study. The results for velocity, stress, pressure and state variable show the effectiveness of the stabilized method. The stabilized results for the P1/P1 element compare favorably to the higher order, stable, P2/P1 element, but require an order of magnitude fewer degrees of freedom. Thus, significant computational savings are realized by using stabilized P1/P1 elements. The P1/P1 element without stabilization gives poor results, as expected.

ACKNOWLEDGEMENTS

This work has been supported by the National Science Foundation through grant DMI-9634920 as well as by the U.S. Department of Defense—Department of the Air Force, Wright Laboratory.

REFERENCES

1. Dawson PR. On modeling of mechanical property changes during flat rolling of aluminum. *International Journal of Solids and Structures* 1987; **23**:947–968.
2. Kobayashi S, Oh S, Altan T. *Metal Forming and the Finite Element Method*. Oxford University Press: New York, 1989.
3. Maniatty AM, Chen M. Shape sensitivity analysis for steady metal forming processes. *International Journal for Numerical Methods in Engineering* 1996; **39**:1199–1217.
4. Brezzi F, Fortin M. *Mixed and Hybrid Finite Element Methods*. Springer: Berlin, 1991.
5. Zienkiewicz OC, Taylor RL. *The Finite Element Method*, *Fourth Edition*, vol. 2. McGraw-Hill: New York, 1991; 438–505.
6. Brezzi F, Franca LP, Hughes TJR, Russo A. Stabilization techniques and subgrid scales capturing. In *The State of the Art in Numerical Analysis*, Duff IS, Watson GA (eds). IMA Conference Series, vol. 63. Oxford University Press: London, 1996; 391–406.
7. Heinrich JC, Zienkiewicz OC. Quadratic finite element schemes for two dimensional convective-transport problems. *International Journal for Numerical Methods in Engineering* 1977; **11**:1831–1844.
8. Brooks AN, Hughes TJR. Streamline upwind/Petrov–Galerkin formulation for convection dominated flows with particular emphasis on the incompressible Navier–Stokes equation. *Computer Methods in Applied Mechanics and Engineering* 1982; **32**:199–259.
9. Hughes TJR, Brooks AN. A theoretical framework for Petrov–Galerkin methods with discontinuous weighting functions. In *Finite Elements in Fluids*, vol. 4, Gallagher RH (ed.). Wiley: Chichester, 1982; 47–65.
10. Donea J, Belytschko T, Smolinski P. A generalized Galerkin method for steady state convection–diffusion problems with application to quadratic shape functions. *Computer Methods in Applied Mechanics and Engineering* 1985; **48**:25–43.
11. Hughes TJR, Franca LP, Hulbert GM. A new finite element formulation for computational fluid dynamics: VIII. The Galerkin/least-squares methods for advective–diffusive equations. *Computer Methods in Applied Mechanics and Engineering* 1989; **73**:173–189.
12. Johnson C, Pitkaranta J. An analysis of the discontinuous Galerkin methods for hyperbolic conservation laws. *Computer Methods in Applied Mechanics and Engineering* 1996; **133**:259–286.
13. Baumann CE, Oden JT. A discontinuous Galerkin hp finite element method for convection–diffusion problems. *Computer Methods in Applied Mechanics and Engineering* 1999; **175**:311–341.

14. Hughes TJR, Franca LP, Balestra M. A new finite element formulation for computational fluid dynamics: V. Circumventing the Babuska–Brezzi condition: a stable Petrov–Galerkin formulation of the Stokes problem accommodating equal-order interpolations. *Computer Methods in Applied Mechanics and Engineering* 1985; **59**:85–99.
15. Franca LP, Hughes TJR, Loula AFD, Miranda I. A new family of stable elements for nearly incompressible elasticity based on a mixed Petrov–Galerkin finite element method. *Numerical Mathematics* 1988; **53**:123–141.
16. Klaas O, Maniatty AM, Shephard MS. A stabilized mixed finite element methods for finite elasticity. *Computer Methods in Applied Mechanics and Engineering* 1999; **180**:65–79.
17. Maniatty AM, Liu Y, Klaas O, Shephard MS. Stabilized finite element method for viscoplastic flow: formulation and a simple progressive solution strategy. *Computer Methods in Applied Mechanics and Engineering* 2001; **190**:4609–4625.
18. Franca LP, Frey S, Hughes TJR. Stabilized finite element methods: I. Application to the advective–diffusive model. *Computer Methods in Applied Mechanics and Engineering* 1992; **99**:209–233.
19. Jansen KE, Collis SS, Whiting C, Shakib F. A better consistency for low-order stabilized finite element methods. *Computer Methods in Applied Mechanics and Engineering* 1999; **174**:153–170.
20. Brown SB, Kim KH, Anand L. An internal variable constitutive model for hot working of metals. *International Journal of Plasticity* 1989; **5**:95–130.
21. Eggert GM, Dawson PR, Mathur KK. An adaptive descent method for non-linear viscoplasticity. *International Journal for Numerical Methods in Engineering* 1991; **31**:1031–1054.
22. Beall MW, Shephard MS. An object-oriented framework for reliable numerical simulations. *Engineering with Computers* 1999; **15**:61–72.
23. Christie I, Griffiths DF, Mitchell AR, Zienkiewicz OC. Finite element methods for second order differential equations with significant first derivatives. *International Journal for Numerical Methods in Engineering* 1976; **10**:1289–1396.

